RESEARCH ARTICLE | APRIL 24 2026

Self-aligned patterning by area-selective etching of polymers and area-selective atomic layer deposition: Decreasing polymer flow and activating noncatalytic surface

Special Collection: Area Selective Deposition

Valtteri Lasonen ; Piyumi Liyana Pathiranage ; Mykhailo Chundak ; Marko Vehkamäki ; Matthias Carnoy ; Benjamin Borie; Silvia Armini ; Mikko Ritala

J. Vac. Sci. Technol. A 44, 032411 (2026)
https://doi.org/10.1116/6.0005294

JVST A
Journal of Vacuum Science & Technology A

ARTICLE

pubs.aip.org/avs/jva

Self-aligned patterning by area-selective etching of polymers and area-selective atomic layer deposition: Decreasing polymer flow and activating noncatalytic surface

Cite as: J. Vac. Sci. Technol. A 44, 032411 (2026); doi: 10.1116/6.0005294
Submitted: 9 January 2026 · Accepted: 2 April 2026 ·
Published Online: 24 April 2026

Valtteri Lasonen,[1,a)] Piyumi Liyana Pathiranage,[1] Mykhailo Chundak,[1] Marko Vehkamäki,[1] Matthias Carnoy,[2] Benjamin Borie,[2] Silvia Armini,[3] and Mikko Ritala[1]

AFFILIATIONS

[1]Department of Chemistry, University of Helsinki, A.I. Virtasen aukio 1, Helsinki FIN-00014, Finland
[2]ATLANT 3D, Mårkærvej 2 B, Taastrup DK-2630, Denmark
[3]Imec, Kapeldreef 75, Leuven B-3001, Belgium

Note: This paper is a part of the Special Topic Collection on Area Selective Deposition.
[a)]**Author to whom correspondence should be addressed:** valtteri.lasonen@helsinki.fi

ABSTRACT

Future semiconductor device architectures necessitate innovative patterning processes. Area-selective etching (ASE) of polymers is a self-aligned patterning technique with significant potential for the future semiconductor fabrication. In the ASE process, etchant gas penetrates the polymer film and becomes activated by the underlying catalytic material. Consequently, at the correct temperature, the polymer layer is selectively decomposed above the catalytically active areas, while it remains unaltered above catalytically inactive areas. This area-selective process ensures self-alignment, thus preventing edge placement errors. The resulting patterned polymer can be utilized in subsequent area-selective deposition or lift-off processes. In this article, we study ASE of poly(methyl methacrylate) (PMMA) and poly(lactic acid) by first testing several metal oxide and nitride surfaces, namely, Al_2O_3, HfO_2, ZrO_2, Ta_2O_5, CeO_2, NiO, TiO_2, TiN, and Si_3N_4, for their catalytic effect in an O_2, H_2, and inert atmosphere. The experiments reveal that most of these surfaces are noncatalytic, therefore requiring activation. We demonstrate that a noncatalytic surface (HfO_2) can be easily converted to catalytic by depositing a small amount of catalytic material (CeO_2) on top. We then create a test structure by patterning another noncatalytic material (TiO_2) on top with direct atomic layer processing, after which we use ASE of PMMA to create a patterned inhibition layer. This inhibition layer is then used in area-selective atomic layer deposition of ZrO_2. Additionally, we show that the polymer flow during the ASE process can be significantly reduced by increasing the molecular weight of the polymer.

I. INTRODUCTION

The number of transistors and other semiconductor devices in integrated circuits has increased drastically over the decades, which has continuously led to more powerful and energy efficient computers.[1] Improvements in lithography have been the most important factor enabling this progress, even though alignment issues have increased. However, future semiconductor device architectures might not be possible to realize with conventional lithography techniques alone because scaling of 2D architectures is reaching its physical limits. Thus, the semiconductor industry has moved toward 3D device architectures. This shift has forced to research and develop alternative film deposition and patterning methods.

Area-selective atomic layer deposition (AS-ALD) is an important emerging method, which shows great potential for enabling the increase in transistor count in integrated circuits to continue.[2–4] In AS-ALD, the deposition occurs only on the desired areas (growth areas), whereas no deposition occurs on the nondesired areas

(nongrowth areas). If the selectivity derives from the different materials exposed on the surface, AS-ALD is self-aligning, thus avoiding alignment errors. There are three main approaches to AS-ALD: inherent, activation, and passivation. In inherent AS-ALD, the selective deposition between different surfaces occurs without any pretreatment or additives.[5–7] Examples of inherently selective processes are many noble metal ALD processes which show large nucleation delay on non-noble metal surfaces. In activated AS-ALD, growth areas are activated enabling deposition to occur on them, whereas nongrowth areas remain unfavorable for the deposition. An example of commonly used strategy for activated AS-ALD is seed-assisted deposition.[8] By far the most common approach to AS-ALD is passivation. In AS-ALD via passivation, the nongrowth areas are passivated against the deposition, while the deposition can occur on the nonpassivated growth areas. The passivation is done by using small molecule inhibitors (SMIs),[9,10] self-assembled monolayers (SAMs),[11,12] or polymers.[13,14] Alternatively, the nongrowth areas can be chemically modified to be inert, e.g., by fluorination.[15,16]

Area-selective etching (ASE) of polymers is a unique method for achieving area-selectivity.[17–19] It is a self-aligning patterning method where a polymer layer is selectively etched via catalytic decomposition only on catalytic surfaces. In ASE, the polymer is first deposited on the whole structure [Fig. 1(a)]. Due to the porosity of many polymers, small gas molecules, such as O_2 and H_2, readily permeate through the polymer [Fig. 1(b)]. When these molecules reach the noncatalytic material, they remain intact. On the contrary, when reaching the catalytic material, the gas molecules are dissociated into reactive atoms. At the correct temperature, the reactive atoms decompose the polymer film only on top of the catalytic material, whereas on top of the noncatalytic material, the polymer stays intact [Fig. 1(c)]. The catalytic polymer decomposition mechanism varies depending on the etchant gas. Combustion occurs when using O_2, and hydrogenolysis when using H_2 as the etchant gas. The catalytic decomposition can also occur without any etchant gas by catalytic cracking.[20–22] In the latter cases, the catalytic effect has been correlated to the Brønsted and Lewis acid sites on the surface. Once the self-aligned decomposition of the polymer is complete and the catalytic surface exposed [Fig. 1(d)], the patterned polymer can be used as an inhibitor in a subsequent AS-ALD process [Fig. 1(e)]. Polymers are excellent inhibitors because they do not necessarily require perfect selectivity. If some undesired film growth occurs on the polymer, removal of the polymer afterward by simple dissolution will remove (lift-off) also the material deposited on the polymer. This is generally not possible with SAMs and SMIs due to their small sizes.

In our previous studies,[17–19] we showed that by carefully choosing the right polymer and atmosphere, several surfaces can be used as either catalytic or noncatalytic. For example, Pt showed excellent catalytic effect in air atmosphere for the decomposition of both poly(methyl methacrylate) (PMMA)[17,18] and poly(lactic acid) (PLA).[19] However, in the presence of H_2, Pt catalytically decomposed only PLA. By contrast, native CuO_x catalytically decomposed PMMA (Ref. 18) but not PLA (Ref. 19) in an inert atmosphere and in the presence of H_2. Many surfaces did not show any catalytic effect in any of the atmospheres. Our experiments have shown, however, that already a small amount, less than

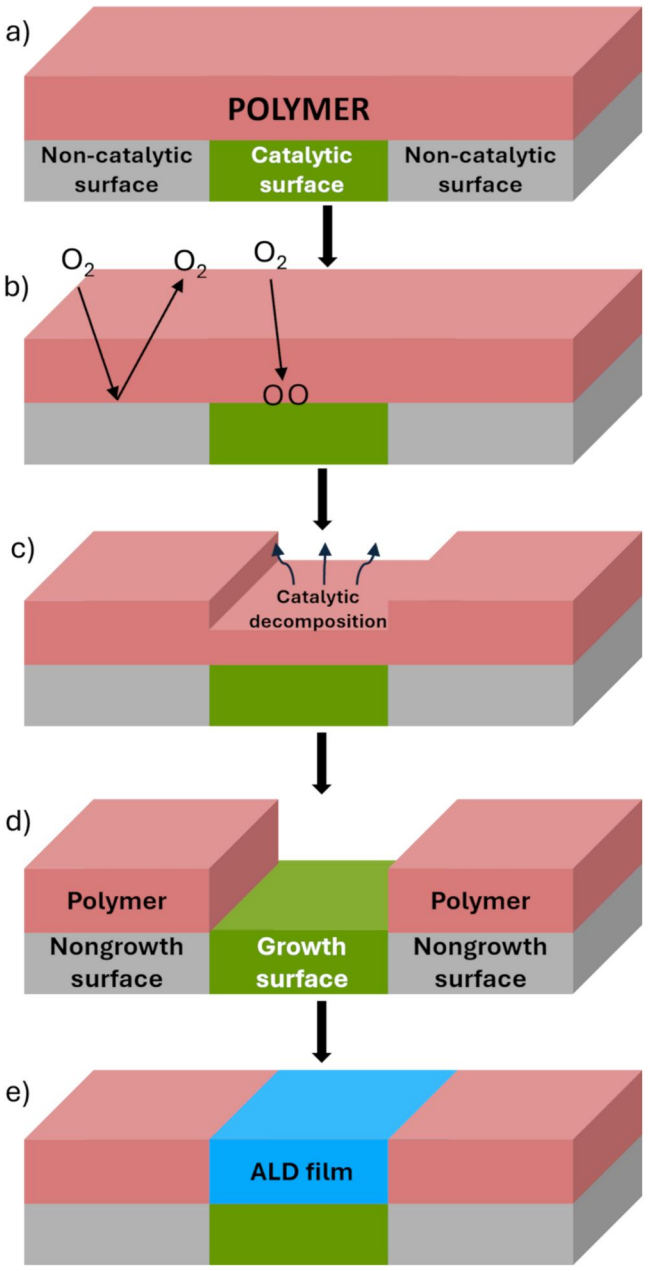

FIG. 1. Schematic depiction of ASE of polymers via catalytic combustion followed by area-selective atomic layer deposition. (a) Polymer film deposited on a substrate with catalytic and noncatalytic surfaces. (b) Diffusion of O_2 molecules through the polymer and their dissociation into atomic oxygen on the catalytic surface, while on the noncatalytic surface O_2 molecules stay unchanged. (c) The reactive oxygen atoms combust the polymer only on the catalytic surface. (d) The catalytic combustion of the polymer exposes the catalytic surface while the polymer on the noncatalytic surface stays intact. (e) After the ASE step, the patterned polymer can be exploited, for example, in the AS-ALD process.

a monolayer, of the catalytic material, e.g., Pt or CeO_2, is enough to activate the catalytic decomposition of polymers.[18] This means that noncatalytic metal surfaces can be converted to catalytic by depositing only a small amount of Pt, and noncatalytic dielectric surfaces are made catalytic by adding a small amount of CeO_2.

Good patterning resolution was achieved with ASE of polyimide[17] and PMMA[18] although noticeable polymer flow occurred with PMMA because temperatures above its melting point had to be used. The polymer flow was significant in ASE of PLA which caused poor patterning resolution.[19] However, we demonstrated that the PLA flow can be reduced by using more crystalline PLA, likely due to its higher melting point. The semicrystalline PLA also showed better Cu-ALD inhibition properties and remained intact during the Cu-ALD, whereas amorphous PLA was degraded.

In this work, we study multiple metal oxide and nitride surfaces for their catalytic effect in the decomposition of PMMA and PLA. Both the polymers used in this study are commercially available, nontoxic, and environmentally friendly.[23,24] The oxide surfaces studied are Al_2O_3, HfO_2, ZrO_2, Ta_2O_5, CeO_2, NiO, and amorphous and crystalline TiO_2. The nitride surfaces studied are TiN and Si_3N_4. We show that most of these surfaces are noncatalytic, but we can convert them to catalytic by depositing a small amount of CeO_2. We demonstrate this by converting a noncatalytic HfO_2 surface to catalytic with 30 ALD cycles of CeO_2 (<1 nm in thickness), after which we pattern another noncatalytic material, amorphous TiO_2, on top. We then spin-coat PMMA film on top of this structure and use ASE to pattern the PMMA. Finally, we use AS-ALD of ZrO_2 on $HfO_2(CeO_2)$ versus PMMA/TiO_2 to demonstrate the feasibility of the whole process. These experiments show that already a thin film (~3.5 nm) of the noncatalytic TiO_2 is enough to deactivate the catalytic effect. Also, we show that by increasing the molecular weight of the PMMA, we can drastically decrease the polymer flow when using Pt as a catalytic surface.

II. EXPERIMENT

A. Preparation and characterization of surfaces for testing

All the tested surfaces were used as-deposited and air-exposed. Air exposure was unavoidable because PMMA and PLA thin films were spin-coated in air. No cleaning or other pretreatment was used, apart from removing dust particles with a nitrogen blow, unless otherwise noted. Film thicknesses were measured by ellipsometry and energy-dispersive x-ray spectroscopy (EDS). Ellipsometry measurements were done with a Film Sense FS-1 multiwavelength ellipsometer. EDS spectra were measured with a Hitachi S-4800 field emission scanning electron microscope (FESEM) equipped with an Oxford INCA 350 EDS spectrometer, and the thicknesses were calculated from the EDS results using a GMRFILM program.[25] An electron beam acceleration voltage of 20 kV was used when measuring the film thicknesses. The Hitachi S-4800 FESEM was also used for scanning electron microscopy (SEM) imaging. Crystalline phases of the thin films were identified by using a PANalytical X'Pert Pro MPD x-ray diffractometer. Cu K_α ($\lambda = 1.54$ Å) radiation with a grazing incidence geometry were used. PANalytical Highscore Plus 4.1 software was used for analyzing the results.

Al_2O_3, HfO_2, ZrO_2, Si_3N_4, and TiN coated silicon wafers were obtained from ASM Microchemistry with film thicknesses around 8–10 nm, as measured with the EDS. TiO_2, CeO_2, NiO, and Ta_2O_5 thin films were deposited on Si(100) substrates by ALD using an F-120 ALD reactor (ASM Microchemistry). Nitrogen (5.0) was used both as a carrier and a purging gas, and the pressure was approximately 10 mbar during all the depositions. TiO_2 films were deposited from $TiCl_4$ and H_2O.[26] Amorphous TiO_2 films were obtained at a deposition temperature of 120 °C and crystalline TiO_2 (anatase) at 300 °C. CeO_2 films were deposited using $Ce(thd)_4$ (thd = 2,2,6,6-tetramethyl-3,5-heptanedionate) (Volatec Oy) and O_3 at 250 °C.[27] NiO films were deposited from bis(*N*,*N*′-di*tert*-butylacetamidinato)nickel(II) (Strem) and H_2O at 150 °C.[28] Ta_2O_5 films were deposited from $Ta(OC_2H_5)_5$ and H_2O at 325 °C.[29]

B. Deposition of polymer films

PLA ($M_w = 40\,000 - 80\,000$ g mol^{-1}, Biosynth) films were deposited by dissolving the polymer in acetonitrile and PMMA thin films by dissolving in toluene and then spin-coating in air using a P-6000 Spin Coater from Specialty Coating Systems, Inc. Three different molecular weights (weight average, M_w) of PMMA were used: $M_w = 15\,000$ (Sigma Aldrich), 550 000 (Alfa Aesar), and 996 000 (Sigma Aldrich) g mol^{-1}. After the spin-coating, the PMMA and PLA samples were baked in air for 1 h at 100 and 60 °C, respectively, to remove the remaining solvent. All the tested surfaces were measured and modeled by an ellipsometer before the spin-coating. After the spin-coating, the polymer film thicknesses and the refractive indices were measured and modeled as Cauchy layers by an ellipsometer. The refractive indices of PMMA and PLA films were ~1.49 and ~1.46, respectively. After the spin-coating and baking, thicknesses of the PMMA films varied between 80 and 110 nm, and those of the PLA films between 70 and 96 nm. However, all the polymer film thicknesses for the same surface-polymer combination were within 10 nm. Polymer thicknesses at 25 °C presented in the graphs (Figs. 2 and 3) are average polymer thicknesses of the surface-polymer samples after the spin-coating and baking. The thicknesses of the PMMA films on the patterning samples varied between 30 and 40 nm.

C. Decomposition of polymer films on different surfaces

Catalytic effects of all the surfaces were tested in air, in an inert atmosphere (N_2, 99.999%), or in the presence of H_2 (5% H_2/95% Ar) at different temperatures. The air experiments were done in ambient air and isothermal conditions with a Vulcan® 3-550 furnace. The furnace was first heated to the target temperature, and once this was reached, the samples were inserted into the furnace. After the target time, the samples were taken out of the furnace and cooled down at room temperature. No intentional air flow was used but the local ventilation close to the furnace exhaust possibly created a small air flow inside the furnace. Both N_2 and H_2 experiments were done in a leak tight tubular furnace (Carbolite Furnaces CTF 12/75/700) at atmospheric pressure. A special sample holder allowed the movement of the samples between the cold end and the heated zone of the tubular furnace,

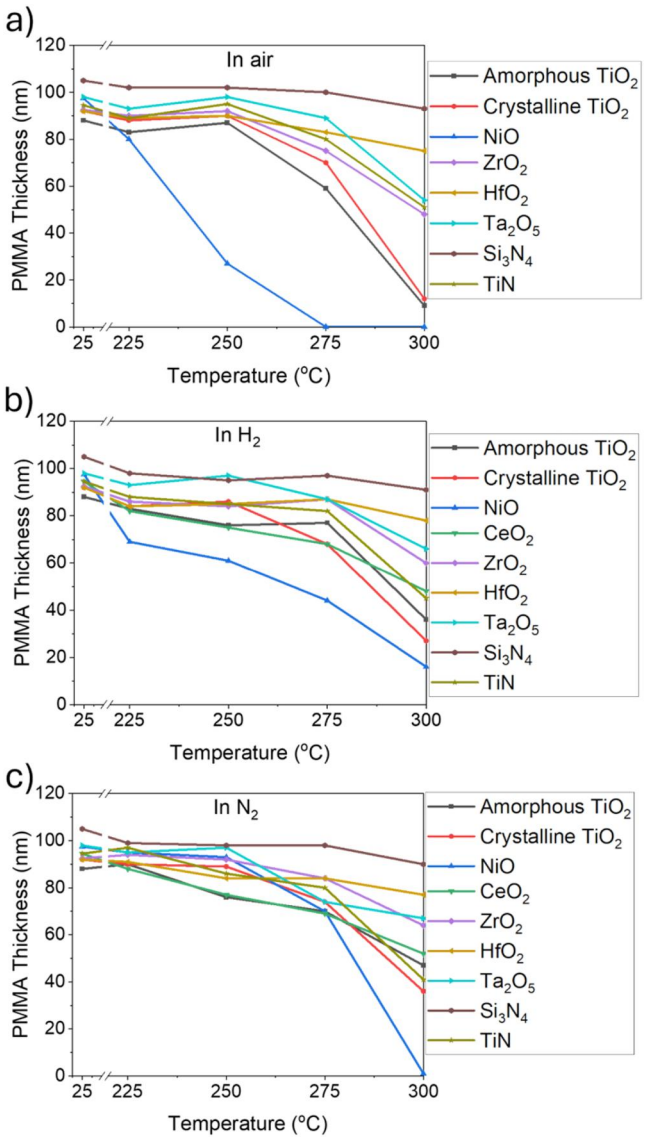

FIG. 2. Thicknesses of PMMA thin films on different surfaces after 120 min at different temperatures (a) in air, (b) in the presence of H_2, and (c) in the inert atmosphere.

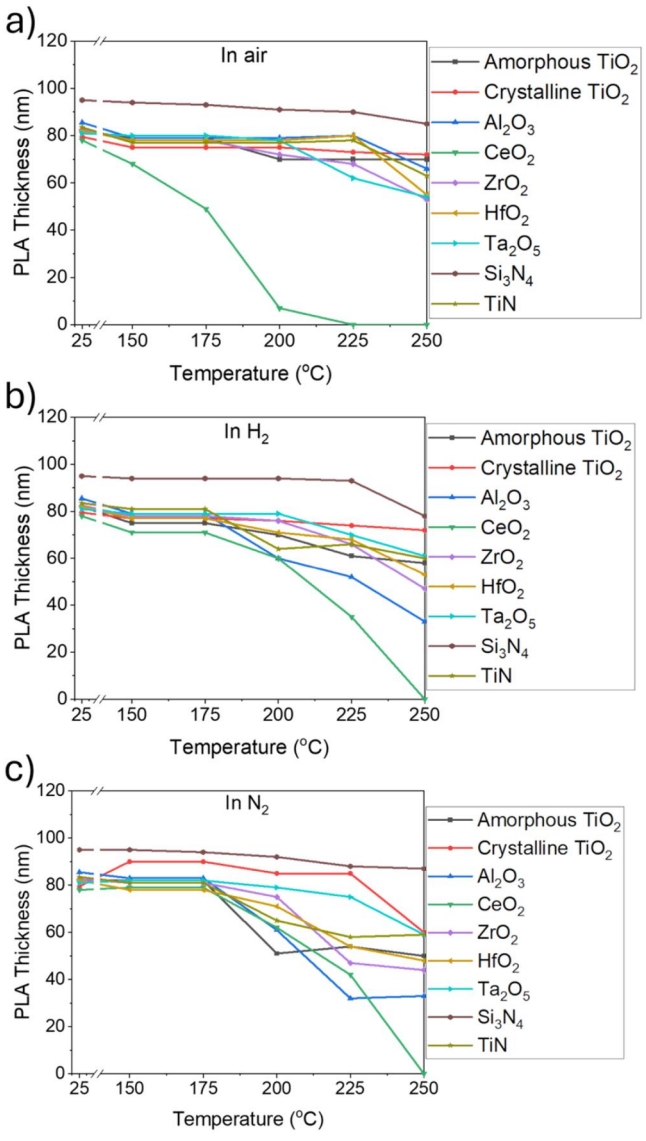

FIG. 3. Thicknesses of PLA thin films on different surfaces after 120 min at different temperatures (a) in air, (b) in the presence of H_2, and (c) in the inert atmosphere.

thus exploiting isothermal conditions within the heated zone. After the samples were inserted into the cold end of the furnace, thorough pumping followed by purging with either N_2 or H_2/Ar gas was conducted to remove all the air from the furnace, after which a minimal gas flow was kept throughout the experiment. The furnace was then heated to the target temperature, and the samples were inserted into the heated zone. After the target time, the samples were retracted into the cold end to cooldown. It is worth mentioning that the cold end was not at room temperature, but, e.g., at less than 90 °C when the heated zone was at 300 °C.

The polymer film thickness change was observed by measuring the thickness before and after the annealing. The polymer film thickness was measured with an ellipsometer using both fixed and fitted refractive indices. The refractive indices changed slightly as the polymer thickness decreased. However, it did not significantly affect the thickness values whether the fixed or the fitted refractive index was used. Therefore, the thicknesses obtained with the fixed refractive indices, i.e., 1.49 for PMMA and 1.46 for PLA, are used in the graphs (Figs. 2 and 3). Some of the results were confirmed by measuring the intensity of the carbon Kα-line (0.277 keV)

using EDS. In our previous studies, the ellipsometry results of PMMA and PLA have been in-line with other characterization methods, namely, EDS, FTIR, and Raman spectroscopy.[18,19]

D. Patterning of low and high molecular weight PMMA by ASE

The effect of the molecular weight of PMMA on the patterning resolution was tested using Pt patterns made on native SiO_2 by the lift-off process. Si wafer with a resist patterned by displacement Talbot lithography[30] was obtained from AlixLabs AB. The resist had a hexagonal array of circular openings of around 200 nm in diameter with a 500 nm pitch. Electron beam evaporation was used to deposit about 20 nm thin film, consisting of a thin Ti adhesion layer followed by a Pt layer, after which the lift-off was finished by dissolving the resist. The patterned samples were characterized by atomic force microscopy (AFM) using a Veeco Multimode V instrument. A Si probe with a nominal tip radius of 10 nm and a spring constant of 40 Nm^{-1} was used to capture images in the air. Images were either flattened (second order) or planefitted (second order) to remove artifacts from the sample tilt and scanner bow. The AFM images and the height profiles were exported using Gwyddion 2.68 software. The patterned Pt/SiO_2 samples were spin-coated with PMMA ($M_w = 15\,000$ and 996 000 g mol^{-1}) and then annealed in air to create the pattern by ASE.

E. Inhibition of ALD-ZrO_2 with PMMA

The inhibition of ALD-ZrO_2 by PMMA ($M_w = 996\,000$ g mol^{-1}) was studied by comparing bare native oxide terminated Si surface and Si surface covered by ~40 nm PMMA film with x-ray photoelectron spectroscopy (XPS) and low-energy ion scattering spectroscopy (LEIS) measurements. ZrO_2 was deposited with a Beneq TFS 200 reactor from tetrakis(ethylmethylamido)zirconium (IV) (TEMAZr) (Sigma Aldrich) and H_2O at 140 °C. The XPS measurements were conducted using a commercial system from PREVAC.[31] The spectra were acquired at 200 eV pass energy with monochromatized Al K_α x-ray source $h\nu = 1487.7$ eV and a hemispherical electron analyzer with a 2D spatial detector. The slits used for the experiments were S2.5 × 25. The pressure in the chamber during the measurements was ~3×10^{-10} mbar. For evaluation of the spectra, CasaXPS software was used. LEIS spectra were measured with an IONTOF Qtac 100 dedicated LEIS instrument. The spectra were collected using 3 keV helium ions, which provide the best available light-element (O and Si) detection and good sensitivity for detecting heavy elements such as Zr.

F. Preparation of activated HfO_2/TiO_2 test structure for the ASE of PMMA

Noncatalytic HfO_2 surface was first converted to catalytic by depositing 30 ALD cycles of CeO_2 from $Ce(thd)_4$ and O_3 at 250 °C. In our previous study, we thoroughly tested the catalytic effect of CeO_2 which showed that even a small amount of CeO_2 is enough for the catalytic effect. Growth per cycle was around 0.3 Å, as measured with EDS, thus the nominal thickness of the CeO_2 film was less than 1 nm. From now on, this CeO_2 coated HfO_2 surface is referred to as $HfO_2(CeO_2)$. After this, four ~350 μm wide amorphous TiO_2 lines were deposited on the $HfO_2(CeO_2)$ surface. The amorphous TiO_2 lines were deposited using ATLANT 3D's Direct Atomic Layer Processing (DALP®)[32] in ALD mode, using the titanium(IV) isopropoxide + H_2O recipe developed on the NANOFABRICATOR™ tool. The deposition was performed at a substrate temperature of 150 °C, and the targeted line thicknesses were 3.5, 14, 24.5, and 35 nm. Profilometry performed across the lines showed results in good agreement with the targeted thicknesses.

G. Self-aligned patterning by ASE of PMMA and AS-ALD of ZrO_2

The patterned $TiO_2/HfO_2(CeO_2)$ sample was spin-coated with PMMA ($M_w = 996\,000$ g mol^{-1}) and annealed in the air to create the pattern by ASE. After the ASE process, ZrO_2 was deposited with 50 cycles of TEMAZr and H_2O at 140 °C. The self-aligned patterning of PMMA and the AS-ALD of ZrO_2 were studied by SEM and measuring the intensity of the carbon Kα-line (0.277 keV) and the zirconium Lα-lines (~2.04 keV) using EDS at an electron beam acceleration voltage of 10 keV. The EDS measurements from the TiO_2 and the $HfO_2(CeO_2)$ regions were measured close to the boundary of these two regions.

III. RESULTS AND DISCUSSION

In our previous works, on a noncatalytic native SiO_2 surface PMMA films showed evident decomposition at 325 °C (Ref. 18) and PLA films at 275 °C.[19] Thus, a surface is considered catalytically active if the polymer film is fully decomposed after annealing for 120 min below these temperatures. The 120 min threshold was chosen because in our previous studies catalytic decomposition in some cases required more than 60 min but no more than 120 min.[17,18] Even though many surfaces were ranked noncatalytic, some of them showed faster decomposition of the polymers as compared to the truly noncatalytic surfaces. It is important to mention, therefore, that such surfaces might be usable as catalytic by increasing either the annealing time or temperature. This is because a minor degradation of a polymer on a noncatalytic surface is acceptable if the polymer can still inhibit the subsequent deposition. Additionally, it is worth noting that the polymers are heated well above their glass transition temperatures, thus some densification might occur during the annealing explaining minor decreases in thicknesses even on noncatalytic surfaces.

A. Catalytic effects of metal oxide and nitride films

In our previous works, CeO_2 and the native CuO_x promoted the decomposition of PMMA films,[18] and CoO and NiO promoted the decomposition of PLA films.[19] Therefore, in this study, several other metal oxide films, namely, TiO_2, HfO_2, ZrO_2, and Ta_2O_5, were tested. Additionally, NiO was tested with PMMA, and CeO_2 and Al_2O_3 with PLA. Also, important nitrides used in semiconductor devices, Si_3N_4 and TiN, were tested with both polymers.

Neither of the TiO_2 surfaces, amorphous or crystalline, showed good catalytic effect in the decomposition of PMMA in any of the atmospheres (Fig. 2) although the decomposition was evident at 300 °C, as compared to some other surfaces such as Si_3N_4 and HfO_2. Similarly, ZrO_2, Ta_2O_5, and TiN showed no evident catalytic effect in the decomposition of PMMA in any of the atmospheres. Our previous experiments demonstrated that CeO_2 shows catalytic effect already at 250 °C in air.[18] Unlike in the air, CeO_2 did not show any catalytic effect in the inert atmosphere or in the presence of H_2 [Figs. 2(b) and 2(c)]. NiO showed excellent catalytic effect in air and some catalytic effect both in the inert atmosphere and with H_2. However, the decomposition was not complete in 120 min at 300 °C with H_2. It is unclear why the decomposition of PMMA is complete in the inert atmosphere but not in the presence of H_2. A possible explanation is that the NiO film gets reduced by H_2, thus stopping the catalytic effect of the oxide. A similar effect was previously observed with Cu/CuO_x and Co/CoO_x.[18,19] However, in our previous work,[19] NiO showed excellent catalytic effect with PLA in the presence of H_2 but not in the inert atmosphere. This is most likely because condensation polymers, such as polyesters, are highly susceptible to hydrogenolysis.[33,34] In conclusion, only NiO and CeO_2 in the air, and NiO in the inert atmosphere can be ranked catalytic in the decomposition of PMMA. Although both amorphous and crystalline TiO_2 were ranked noncatalytic, they were able to accelerate the decomposition of PMMA.

None of the tested surfaces, other than CeO_2, showed evident catalytic effect in the decomposition of PLA (Fig. 3) in any of the

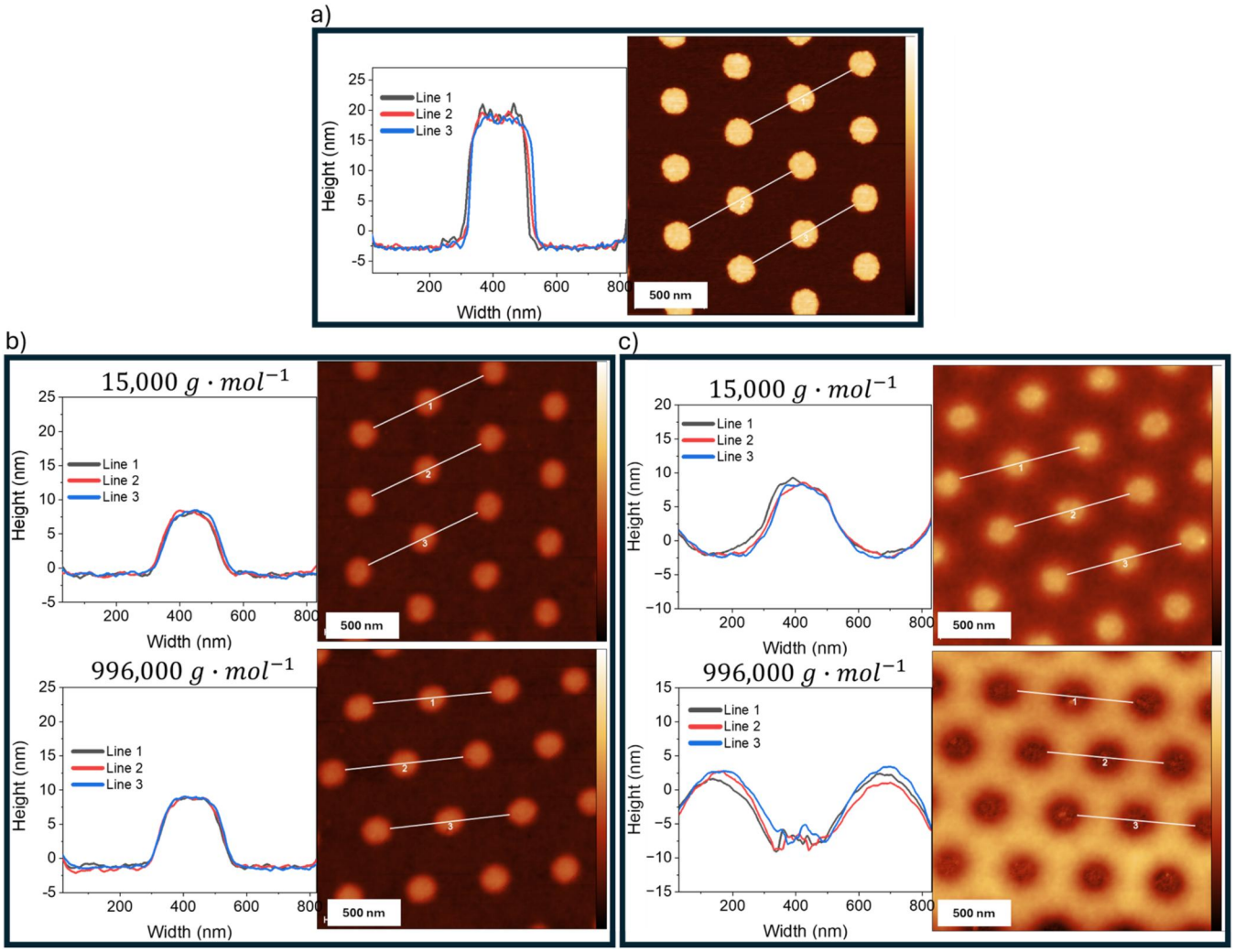

FIG. 4. (a) AFM images and three height profiles (lines 1–3) measured on (a) the bare Pt dot structure, (b) the Pt dot structure after spin-coating with 15 000 and 996 000 g . mol^{-1} PMMA, and (c) the Pt dot structure after ASE of 15 000 and 996 000 g . mol^{-1} PMMA in air at 200 °C for 120 min.

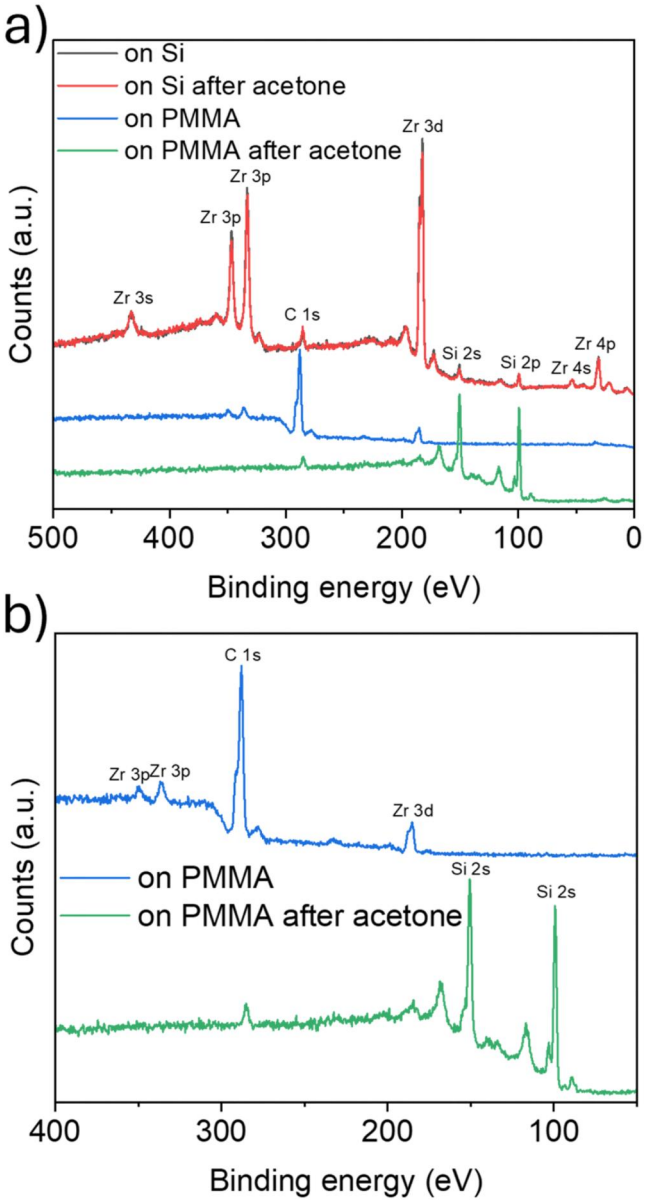

FIG. 5. XPS widescan spectra in a binding energy range of (a) 500–0 and (b) 400–50 eV after 50 cycles of ZrO_2 on native oxide terminated Si, native oxide terminated Si after acetone immersion, PMMA, and PMMA after acetone immersion.

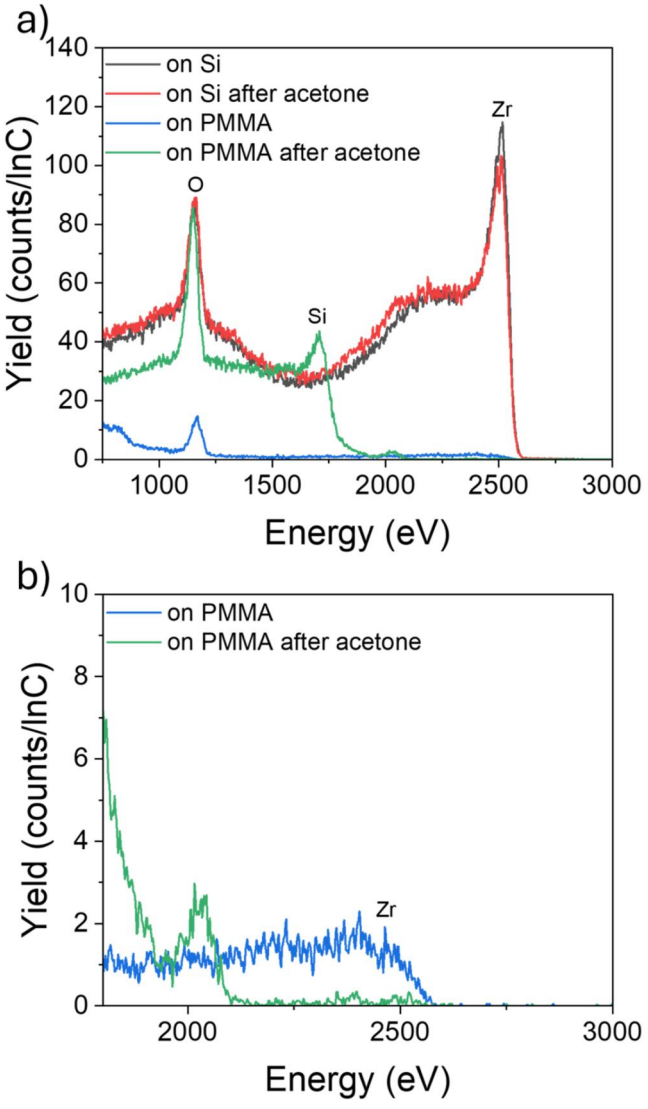

FIG. 6. LEIS (3 keV He) spectra in an energy range of (a) 750–3000 and (b) 1750–3000 eV after 50 cycles of ZrO_2 on native oxide terminated Si, native oxide terminated Si after acetone immersion, PMMA, and PMMA after acetone immersion.

atmospheres. Some surfaces, like Al_2O_3 and ZrO_2, showed some promising results in the inert atmosphere and/or in the presence of H_2 at 225 and 250 °C [Figs. 3(b) and 3(c)]. The decomposition of PLA was evident but not complete at these temperatures. The reason for this decomposition is unclear. Since none of these surfaces was able to fully decompose the PLA films at 250 °C or lower in 120 min, they were ranked noncatalytic. The CeO_2 surface showed excellent catalytic effect in all the atmospheres. In air, the decomposition of PLA on CeO_2 was complete at 225 °C, and in the inert atmosphere and in the presence of H_2 at 250 °C. This demonstrates that CeO_2 can be used as a catalytic surface with PLA as well.

These results show that many materials used in semiconductor devices are inherently noncatalytic for the polymer decomposition. Therefore, to use them as growth surfaces in AS-ALD via ASE, they first must be converted to catalytic. It is important to note that some of the tested surfaces did show faster polymer decomposition than the others at the temperatures where also the

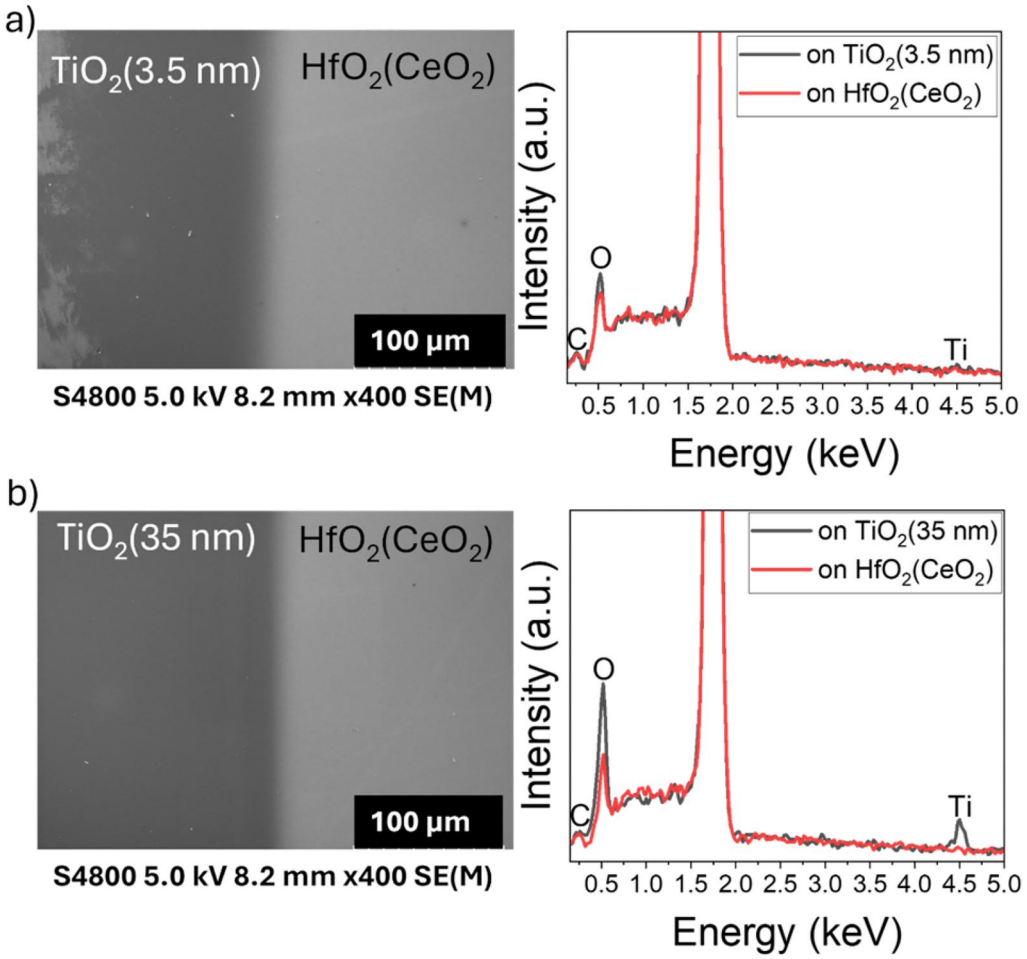

FIG. 7. SEM images and EDS spectra of the $TiO_2/HfO_2(CeO_2)$ structure at (a) the thinnest and (b) thickest TiO_2 line.

noncatalytic decomposition takes place. It is, however, unclear whether these surfaces can be used as catalytic surfaces without first converting them to catalytic.

B. ASE of low vs high molecular weight PMMA

Previously, we demonstrated that increasing the crystallinity of the polymer improves the resolution of the patterning by ASE.[19] This is due to the higher melting points of more crystalline polymers. Increasing the molecular weight can significantly increase the glass transition temperature of the polymer and the viscosity of the polymer melt of amorphous polymers, which should improve the patterning resolution.[35] Resolutions of the ASE-patterned PMMA with different molecular weights ($M_w = 15\,000$ and $996\,000\ g\ mol^{-1}$) were compared using the structure consisting of Pt dots on a Si substrate [Fig. 4(a)].

After spin-coating ~40 nm thick PMMA films, no noticeable difference between the different molecular weight PMMAs was noticed [Fig. 4(b)]. Both 15 000 and $996\,000\ g\ mol^{-1}$ showed ~10 nm high bumps over the Pt dots. Both polymers showed also similar surface roughness.

ASE of PMMA was then done in air at 200 °C for 120 min [Fig. 4(c)]. An evident difference between the different molecular weight PMMA samples was observed. The lower molecular weight sample still showed bumps over the Pt dots as before the annealing [Fig. 4(b)] though the bumps were clearly wider after the annealing. This indicates that the polymer melt flowed during the process, making the patterning by ASE impossible. The higher molecular weight PMMA, by contrast, showed minimal flow during the process and the bumps were converted into dips because of the polymer removal from top of the Pt dots [Fig. 4(c)]. The height difference between the Pt dots and the highest point of the surrounding PMMA film was almost 10 nm. Because the height of the Pt dots was 20 nm, the maximum PMMA thickness on the Si area was around 30 nm. Therefore, the PMMA thickness had decreased by only about 10 nm on the noncatalytic Si surface during the ASE process.

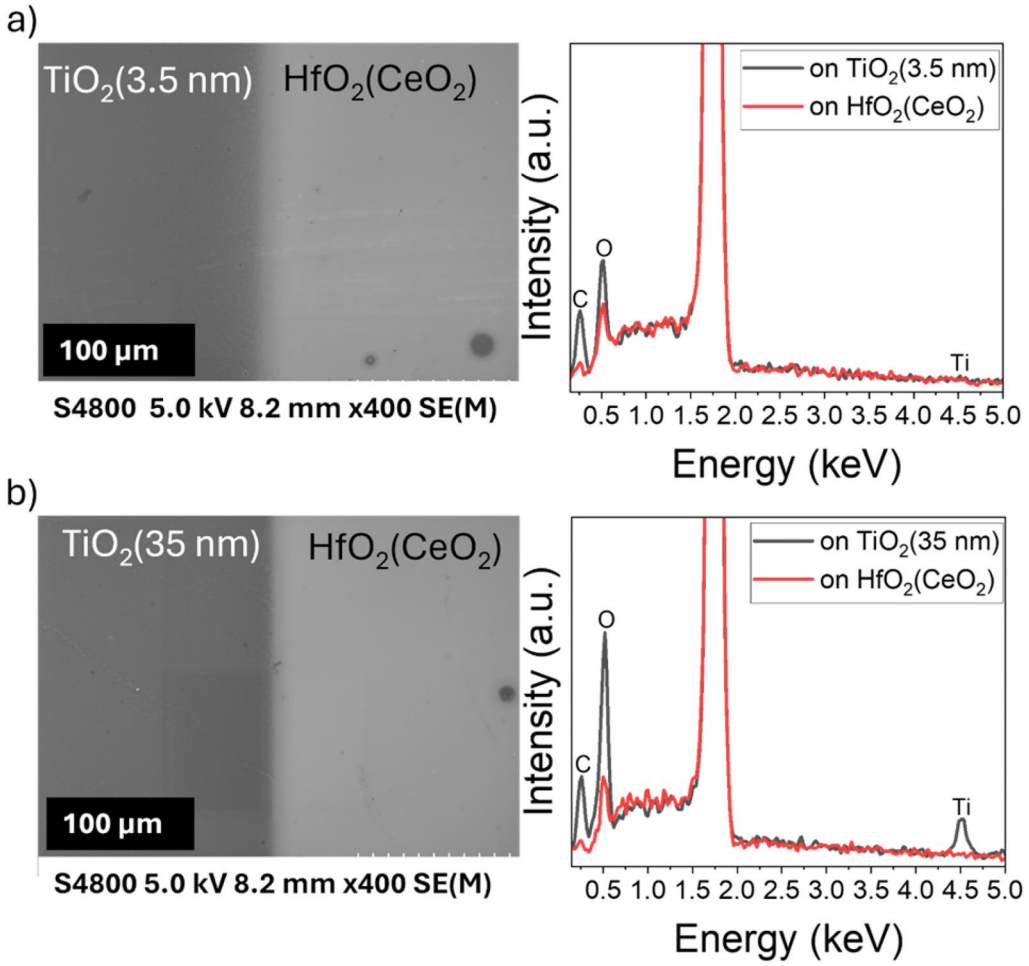

FIG. 8. SEM images and EDS spectra of the $TiO_2/HfO_2(CeO_2)$ structure after ASE of PMMA at 250 °C for 120 min at (a) the thinnest and (b) thickest TiO_2 line.

C. Inhibition of ALD-ZrO_2 with PMMA

ALD growth inhibiting properties of PMMA were tested by exposing native oxide terminated Si and PMMA-coated (~40 nm) Si samples to 50 cycles of TEMAZr and H_2O at 140 °C. After the ZrO_2 ALD, some of the Si and PMMA samples were immersed in acetone overnight and were then rinsed with isopropanol and de-ionized water. The thicknesses of ZrO_2 films on the Si substrates were around 5 nm, as measured with ellipsometry. Four different ZrO_2-ALD samples were then measured with XPS (Fig. 5) and LEIS (Fig. 6): Si, Si immersed in acetone, PMMA on Si, and PMMA on Si immersed in acetone.

Prominent Zr peaks were visible on both Si and Si immersed in acetone samples, as measured with XPS (Fig. 5) and LEIS (Fig. 6). On both Si samples, small peaks from the Si substrate were visible in XPS at ~100 eV (Si 2p) and ~150 eV (Si 2s) (Fig. 5). On the PMMA sample, only small peaks at ~330–350 eV (Zr 3p) and ~180–190 eV (Zr 3d) were visible in XPS, indicating that a small amount of TEMAZr had reacted on/in the PMMA film. When the PMMA was dissolved in acetone, none of the Zr peaks were visible but the Si peaks were prominent. The peaks at ~167 and ~185 eV are due to plasmon loss feature from Si 2s photoelectrons.[36] Similar plasmon loss feature from Si 2p photoelectrons can be seen at binding energies of ~117 and ~135 eV. This shows that TEMAZr did not react with the Si surface underneath the PMMA film. This was confirmed with LEIS (3 keV He) that showed a small amount of Zr (~2500 eV) on the PMMA sample, while Zr was below the detection limit after dissolving the PMMA film in acetone (Fig. 6). A small amount of unidentified contamination was visible at ~2000–2100 eV on the Si surface after the PMMA film was dissolved in acetone (Fig. 6).

D. Self-aligned patterning by ASE of PMMA and AS-ALD of ZrO_2

Patterning by ASE of PMMA followed by AS-ALD of ZrO_2 was studied with ~350 μm wide TiO_2 lines deposited on the

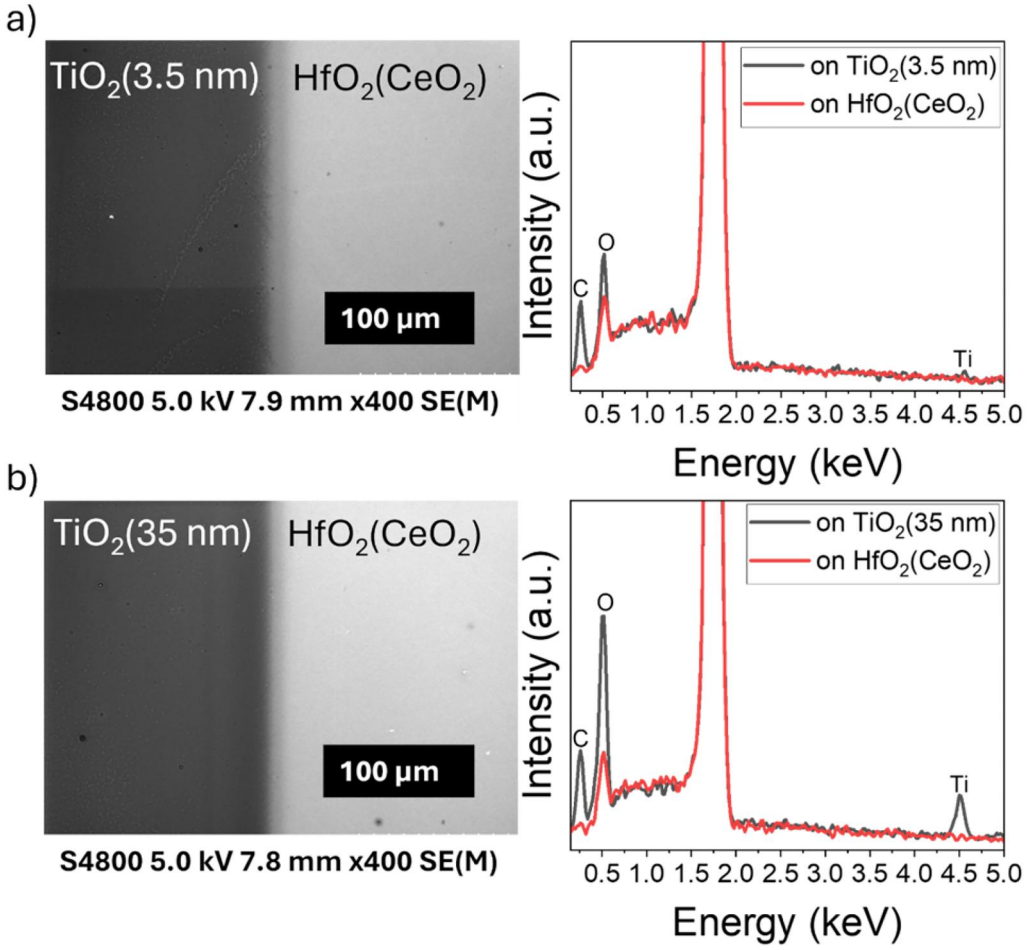

FIG. 9. SEM images and EDS spectra of the $TiO_2/HfO_2(CeO_2)$ structure after ASE of PMMA at 275 °C for 60 min at (a) the thinnest and (b) thickest TiO_2 line.

$HfO_2(CeO_2)$ surface. These structures were made by depositing first 30 ALD cycles of CeO_2 (<1 nm) on HfO_2 and then depositing TiO_2 locally by DALP. DALP enabled straightforward patterning of the TiO_2 lines with different thicknesses (3.5–35 nm) on the $HfO_2(CeO_2)$ surface without any complicated lithography steps. EDS measurements revealed that Ti (Kα-line at ~4.5 keV) was below the detection limit when measured on the 3.5 nm thick TiO_2 line [Fig. 7(a)], but a prominent Ti peak was detected on the 35 nm thick TiO_2 line [Fig. 7(b)]. No Ti was detected when measured on the $HfO_2(CeO_2)$ surface. All the TiO_2 and the $HfO_2(CeO_2)$ surfaces showed small carbon peaks due to carbon contamination. SEM images (Fig. 7) showed that the edges of the TiO_2 lines are not perfectly sharp, preventing the assessment of the ASE-patterning resolution. It is also important to note that defects, such as small unidentified particles and scratches, were visible on both the $HfO_2(CeO_2)$ and TiO_2 surfaces.

The $TiO_2/HfO_2(CeO_2)$ structure was spin-coated by ~40 nm thick PMMA (996 000 g mol^{-1}) film and then annealed in air. Two temperatures, 250 and 275 °C, were tested. SEM images and EDS measurements showed that 120 min at 250 °C was enough to decompose the PMMA from top of $HfO_2(CeO_2)$, whereas PMMA clearly remained on the TiO_2 surface (Fig. 8). Additionally, 3.5 nm [Fig. 8(a)] and 35 nm [Fig. 8(b)] of TiO_2 worked equally well in deactivating the catalytic decomposition. A small amount of carbon was detected on $HfO_2(CeO_2)$, which could either be hydrocarbon contamination from the atmosphere or residue of the decomposed PMMA. Also, some darker spots on the $HfO_2(CeO_2)$ surface were visible in the SEM images, which indicates incomplete decomposition of the PMMA film. However, similar dark spots were also visible on the $HfO_2(CeO_2)$ surface before the PMMA deposition, albeit not as large or numerous (Fig. 7).

Annealing at 275 °C for 60 min gave similar results. According to SEM and EDS, the PMMA film was fully decomposed on the $HfO_2(CeO_2)$ surface while PMMA was again detected on the TiO_2 surfaces, both 3.5 and 35 nm (Fig. 9). This time less defects on the $HfO_2(CeO_2)$ surface were visible in SEM and the

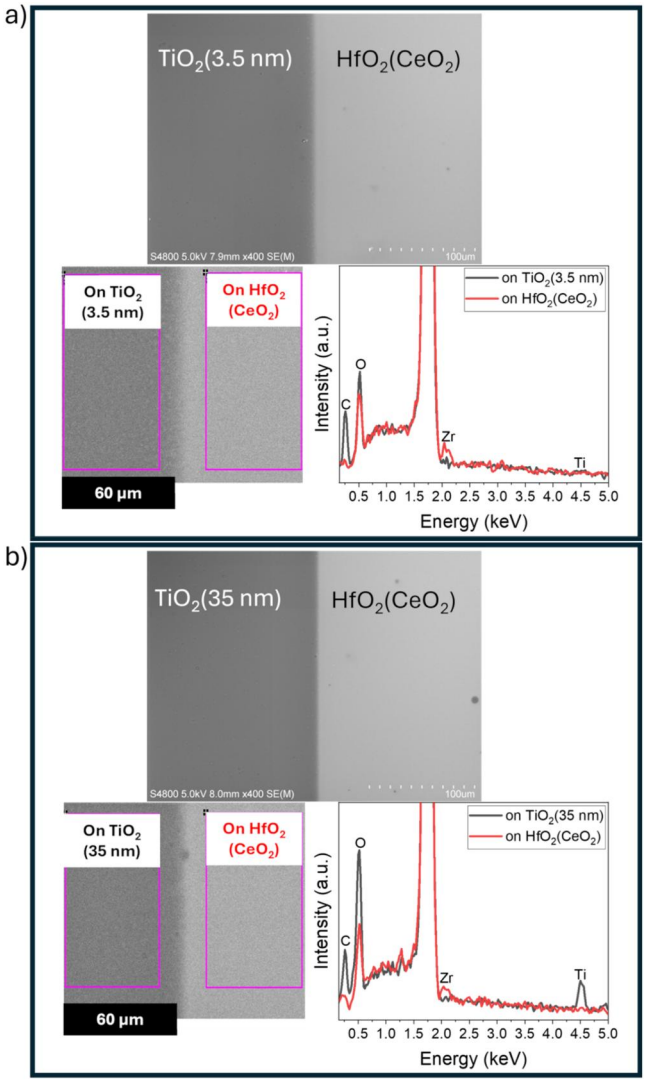

FIG. 10. SEM images and EDS spectra of the $TiO_2/HfO_2(CeO_2)$ structure after ASE of PMMA at 250 °C for 120 min followed by AS-ALD of ZrO_2 at (a) the thinnest and (b) thickest TiO_2 line.

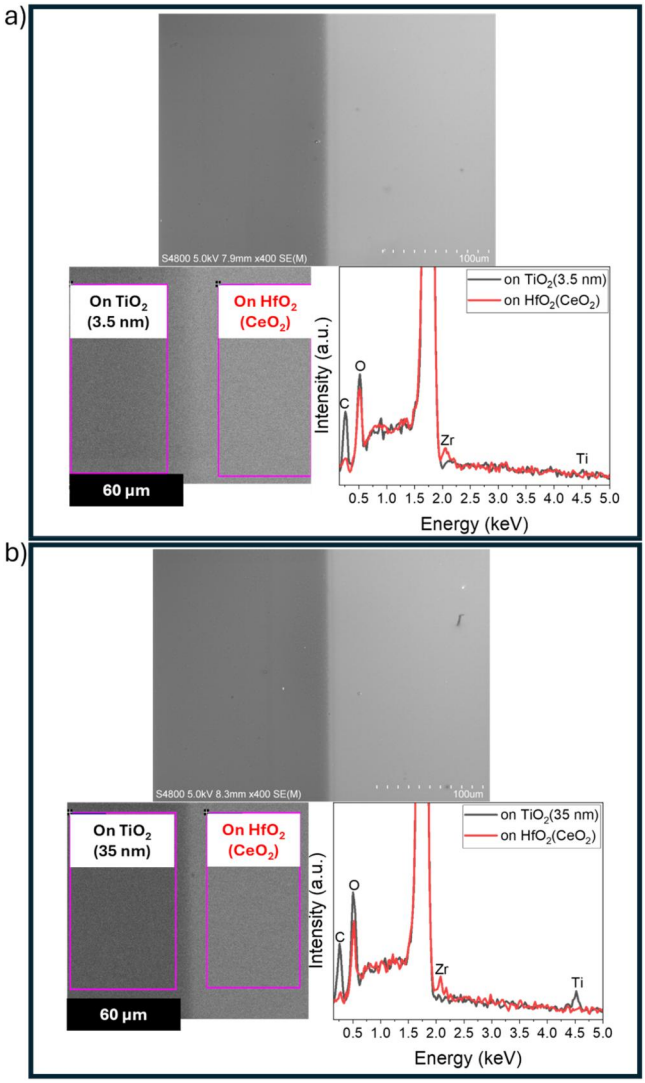

FIG. 11. SEM images and EDS spectra of the $TiO_2/HfO_2(CeO_2)$ structure after ASE of PMMA at 275 °C for 60 min followed by AS-ALD of ZrO_2 at (a) the thinnest and (b) thickest TiO_2 line.

intensity of the carbon peak in the EDS spectrum was miniscule. This shows that residues on the catalytic surface can be decreased by increasing the ASE temperature.

After the ASE of PMMA on the $TiO_2/HfO_2(CeO_2)$ samples, ALD-ZrO_2 was performed at 140 °C using 50 cycles of TEMAZr and H_2O (Figs. 10 and 11). EDS measurements showed prominent Zr peaks on the $HfO_2(CeO_2)$ surface from both the samples. No Zr was detected on any of the TiO_2 surfaces but prominent C peaks were visible, revealing no major decomposition of the PMMA film during the ZrO_2 ALD (Figs. 10 and 11). Furthermore, both the TiO_2 thicknesses showed similar results, i.e., no ZrO_2 growth, further demonstrating that already a thin film (~3.5 nm) of noncatalytic material is enough to deactivate the catalytic effect leaving enough polymer intact for inhibiting the ALD growth.

IV. SUMMARY AND CONCLUSIONS

We tested several metal oxide and nitride surfaces for their catalytic effect in the decomposition of PMMA and PLA. The results showed that most of the materials are noncatalytic or their usability as a catalytic surface is uncertain. However, a noncatalytic surface can be converted to catalytic by depositing a thin layer of catalytic material. We demonstrated this by converting noncatalytic HfO_2 surface to catalytic by 30 ALD cycles of CeO_2. After

this, a noncatalytic TiO_2 film was patterned on top and the ASE of PMMA was done using this structure, demonstrating the feasibility of the whole process. It was also shown that already a thin layer (~3.5 nm) of noncatalytic material is enough to prevent the catalytic decomposition from occurring.

We also studied the inhibition of ZrO_2 ALD with PMMA on the Si surface by XPS and LEIS. Only a small amount of Zr was detected in/on a ~40 nm thick PMMA after 50 cycles of TEMAZr and H_2O, and when the PMMA was removed, no Zr was detected on the Si surface, further demonstrating the excellent inhibition properties of PMMA. AS-ALD of ZrO_2 on $HfO_2(CeO_2)$ versus TiO_2 was demonstrated by ASE of PMMA, followed by 50 cycles of TEMAZr and H_2O (~5 nm thick ZrO_2).

Finally, we showed that the polymer flow during the ASE process can be greatly reduced by increasing the molecular weight of the polymer.

ACKNOWLEDGMENTS

The authors thank the Research Council of Finland (Decision No. 338707) for funding this research. Mykhailo Chundak acknowledges the funding from the Jane and Aatos Erkko Foundation by the project "Novel materials for energy efficient microelectronics." V.L. gratefully thanks Doctoral Programme in Materials Research and Nanoscience (MATRENA), Alfred Kordelin Foundation's Gust. Komppa fund, and Finnish foundation for technology promotion for the personal grants. Paavo Porri and Miika Mattinen are thanked for the help with AFM. V.L. would like to give special thanks to Annelies Delabie from KU Leuven and imec. Without you my research visit at imec would not have happened. The authors thank all the collaborators for their invaluable support during the research of this article: Eva Tois from ASM Microchemistry, Jonas Sundqvist from AlixLabs, and Maksym Plakhotnyuk and Mira Baraket from ATLANT3D. ASM Microchemistry is gratefully acknowledged for providing the substrates, and AlixLabs is gratefully acknowledged for providing the Si substrates with a patterned resist. The work was done at the ALD Center of Finland research infrastructure.

AUTHOR DECLARATIONS

Conflict of Interest

The authors have no conflicts to disclose.

Author Contributions

Valtteri Lasonen: Conceptualization (equal); Data curation (lead); Formal analysis (lead); Investigation (lead); Writing – original draft (lead); Writing – review & editing (lead). **Piyumi Liyana Pathiranage:** Data curation (equal); Formal analysis (equal); Investigation (equal); Writing – review & editing (supporting). **Mykhailo Chundak:** Data curation (supporting); Formal analysis (supporting); Investigation (supporting); Writing – review & editing (supporting). **Marko Vehkamäki:** Data curation (supporting); Formal analysis (supporting); Investigation (supporting); Writing – review & editing (supporting). **Matthias Carnoy:** Data curation (supporting); Formal analysis (supporting); Investigation (supporting); Writing – review & editing (supporting). **Benjamin Borie:** Data curation (supporting); Formal analysis (supporting); Investigation (supporting); Writing – review & editing (supporting). **Silvia Armini:** Conceptualization (supporting); Data curation (supporting); Formal analysis (supporting); Project administration (supporting); Supervision (supporting); Writing – review & editing (equal). **Mikko Ritala:** Conceptualization (equal); Data curation (equal); Formal analysis (equal); Funding acquisition (lead); Project administration (lead); Supervision (lead); Writing – original draft (equal); Writing – review & editing (equal).

DATA AVAILABILITY

The data that support the findings of this study are available from the corresponding author upon reasonable request.

REFERENCES

[1]M. S. Lundstrom and M. A. Alam, Science **378**, 722 (2022).
[2]G. N. Parsons and R. D. Clark, Chem. Mater. **32**, 4920 (2020).
[3]R. Chen, E. Gu, K. Cao, and J. Zhang, Int. J. Mach. Tools Manuf. **199**, 104173 (2024).
[4]A. J. M. Mackus, M. J. M. Merkx, and W. M. M. Kessels, Chem. Mater. **31**, 2 (2019).
[5]C. Zhang, E. Tois, M. Leskelä, and M. Ritala, Chem. Mater. **34**, 8379 (2022).
[6]C. Zhang, M. Vehkamäki, M. Leskelä, and M. Ritala, Dalton Trans. **52**, 9622 (2023).
[7]H.-E. Nieminen, M. Putkonen, and M. Ritala, Chem. Mater. **37**, 7251 (2025).
[8]A. J. M. MacKus, N. F. W. Thissen, J. J. L. Mulders, P. H. F. Trompenaars, M. A. Verheijen, A. A. Bol, and W. M. M. Kessels, J. Phys. Chem. C **117**, 10788 (2013).
[9]J. Yarbrough, A. B. Shearer, and S. F. Bent, J. Vac. Sci. Technol. A **39**, 021002 (2021).
[10]A. Mameli and A. V. Teplyakov, Acc. Chem. Res. **56**, 2084 (2023).
[11]J.-H. Choi, D. G. Kim, S.-H. Lee, K. Choi, W.-H. Kim, C. M. Yoon, and J.-H. Ahn, Mater. Lett. **383**, 138014 (2025).
[12]C. Kim, M. Choi, J. Sim, H. Kim, and C. Choi, Appl. Surf. Sci. **663**, 160033 (2024).
[13]E. Färm, M. Kemell, M. Ritala, and M. Leskelä, J. Phys. Chem. C **112**, 15791 (2008).
[14]E. Färm, M. Kemell, E. Santala, M. Ritala, and M. Leskelä, J. Electrochem. Soc. **157**, K10 (2010).
[15]J. M. Thelven, H. R. M. Margavio, H. Oh, C. M. Efaw, P. H. Davis, E. Graugnard, and G. N. Parsons, Adv. Mater. Technol. **10**, e00284 (2025).
[16]O. C. A. Bolkenbaas, M. J. M. Merkx, N. J. Chittock, I. Tezsevin, W. M. M. Kessels, T. E. Sandoval, and A. J. M. Mackus, Chem. Mater. **37**, 4982 (2025).
[17]C. Zhang, M. Leskelä, and M. Ritala, Coatings **11**, 1124 (2021).
[18]V. Lasonen *et al.*, Chem. Mater. **35**, 6097 (2023).
[19]V. Lasonen, V. Rajamäki, M. Chundak, E. Tois, S. Hietala, and M. Ritala, Chem. Mater. **36**, 11645 (2024).
[20]P. Dwivedi, P. K. Mishra, M. K. Mondal, and N. Srivastava, Heliyon **5**, e02198 (2019).
[21]R. Miandad, M. A. Barakat, A. S. Aburiazaiza, M. Rehan, and A. S. Nizami, Process Saf. Environ. Prot. **102**, 822 (2016).
[22]Y.-H. Lin and M.-H. Yang, J. Appl. Polym. Sci. **114**, 2591 (2009).
[23]S. Teixeira, K. M. Eblagon, F. Miranda, M. F. R. Pereira, and J. L. Figueiredo, C **7**, 42 (2021).
[24]F. Rahman, D. J. Carbaugh, J. T. Wright, P. Rajan, S. G. Pandya, and S. Kaya, Microelectron. Eng. **224**, 111238 (2020).
[25]R. A. Waldo, in *Microbeam Analysis*, edited by D. E. Newbury (San Francisco, San Francisco, CA, 1988), p. 310.
[26]E.-L. Lakomaa, S. Haukka, and T. Suntola, Appl. Surf. Sci. **60–61**, 742 (1992).

[27]J. Päiväsaari, M. Putkonen, and L. Niinistö, J. Mater. Chem. **12**, 1828 (2002).
[28]R. Zhao, S. Xiao, S. Yang, and X. Wang, Chem. Mater. **31**, 5172 (2019).
[29]K. Kukli, J. Aarik, A. Aidla, H. Siimon, M. Ritala, and M. Leskelä, Appl. Surf. Sci. **112**, 236 (1997).
[30]H. H. Solak, C. Dais, and F. Clube, Opt. Express **19**, 10686 (2011).
[31]H.-E. Nieminen, M. Chundak, M. J. Heikkilä, P. R. Kärkkäinen, M. Vehkamäki, M. Putkonen, and M. Ritala, J. Vac. Sci. Technol. A **41**, 022401 (2023).
[32]S. Santucci, A. Kinikar, Z. Wang, N. S. Ruhela, J. Navne, M. Akbari, A. Mishchenko, M. Baraket, and M. Plakhotnyuk, J. Vac. Sci. Technol. A **43**, 062411 (2025).
[33]J. E. Pickett and D. J. Coyle, Polym. Degrad. Stab. **98**, 1311 (2013).
[34]S. Westhues, J. Idel, and J. Klankermayer, Sci. Adv. **4**, eaat9669 (2018).
[35]T. Lin, Y. Li, J. Wang, and J. You, Polymers **13**, 4138 (2021).
[36]L. J. Webb, E. J. Nemanick, J. S. Biteen, D. W. Knapp, D. J. Michalak, M. C. Traub, A. S. Y. Chan, B. S. Brunschwig, and N. S. Lewis, J. Phys. Chem. B **109**, 3930 (2005).